200 mm Surface and Bulk Acoustic Wave Devices Based on Piezoelectric-On-Insulator Substrate

M. Bousquet[1], A. Joulie[1], C. Hellion[1], M. Sansa[1], J. Delprato[1], P. Perreau[1], G. Enyedi[1], G. Lima[1], J. Guerrero[1], G. Castellan[1], A. Tantet[1], S. Chevallet[1], T. Monniez[1], I. Huyet[2], A. Clairet[3], T. Laroche[3], S. Ballandras[3], A. Reinhardt[1]

[1]*Univ. Grenoble Alpes, CEA-LETI, MINATEC Campus, FRANCE*

[2]*Soitec, Bernin, France*

[3]*Soitec, Besançon, France*

marie.bousquet@cea.fr ; alexandre.reinhardt@cea.fr

***Summary* — The availability of Piezoelectric-On-Insulator (POI) substrates, made of a thin single crystal $LiTaO_3$ film atop a silicon substrate, has promoted the development of innovative Surface and Bulk Acoustic Wave (SAW and BAW) devices. However, these substrates are so far only commercially available in 100 and 150 mm diameter. In this work, we successfully demonstrate acoustic devices based on 200 mm POI substrates. First, we fabricate SAW resonators displaying an electromechanical coupling coefficient of 8.8% at a resonance frequency of 1.6 GHz. Then, we implement Film Bulk Acoustic Resonators (FBAR), integrating buried electrodes and an acoustic isolation structure, which exhibits a single resonance at 2.8 GHz, with an electromechanical coupling coefficient of 8.8% and a quality factor close to 190. Eventually, we show a Solidly Mounted Resonator (SMR) based on a dielectric (AlN/SiO_2) Bragg mirror, which exhibits performances close to AlN-based resonators, *i.e.* a coupling coefficient of 6.1% and a quality factor of 405 at 4 GHz. For the later, a Temperature Coefficient of Frequency (TCF) of -14 and -22 ppm/°C at resonance and antiresonance are obtained respectively. Such TCF values are among the lowest ever reported for $LiNbO_3$ and $LiTaO_3$ BAW resonators. These results offer promising perspectives towards the development of 200 mm SAW and BAW filters based on POI substrates.**

Keywords* — *200 mm, Piezoelectric-On-Insulator (POI), Bulk Acoustic Wave (BAW), Surface Acoustic Wave (SAW)

I. INTRODUCTION

The radiofrequency (RF) filter market has been moving fast in the last ten years with the deployment of the 5th generation of mobile applications (5G), especially in the sub-6 GHz range [1]. In this crowded RF spectrum, RF filters need to continuously improve their performances (*e.g.*, insertion loss, temperature stability, skirt steepness, compactness) while new frequency bands introduce challenges regarding higher operation frequency and larger fractional bandwidths. Two RF filter technologies coexist in the current market (Fig. 1):

(i) Surface Acoustic Wave (SAW), where acoustic waves are excited by interdigitated electrodes on top of a bulk ($LiNbO_3$ or $LiTaO_3$) piezoelectric or a Piezoelectric-On-Insulator (POI) substrate. SAW filters are usually manufactured on 100 or 150 mm wafer production lines [2].

(ii) Bulk Acoustic Wave (BAW) where a thin piezoelectric layer is sandwiched between two electrodes and acoustically isolated from the substrate either by an air gap (FBAR – Film Bulk Acoustic Resonator) or a Bragg mirror (SMR – Solidly Mounted Resonator). Sputtered AlN and its derivatives (e.g., $Al_{1-x}Sc_xN$) is currently the prime material for BAW manufacturers, which operate in 150 or 200 mm production lines [1].

New devices exploiting bulk acoustic waves in single crystal $LiNbO_3$ and $LiTaO_3$ piezoelectric films have recently emerged as promising candidates for wide bandwidth filters in the sub-6 GHz range such as laterally eXcited Bulk Acoustic Resonator (XBAR®) [3], [4], rotated Y-cut $LiNbO_3$ thin film membrane (YBAR) [5], and BAW [6]-[13]. In these materials, the polarization of the acoustic wave (shear or longitudinal wave), its velocity (from 3960 to 7320 m/s) and its electromechanical coupling coefficient (from 5% up to 45%) can be adjusted by a proper choice of the crystal orientation. Up to now, their potentialities have been only demonstrated on 100 mm wafers, due in part to limited wafer size availability.

In this paper, we demonstrate the integration and associated performances of SAW and BAW devices based on 200 mm POI substrates highlighting the potential for wafer size upscaling (Fig. 2).

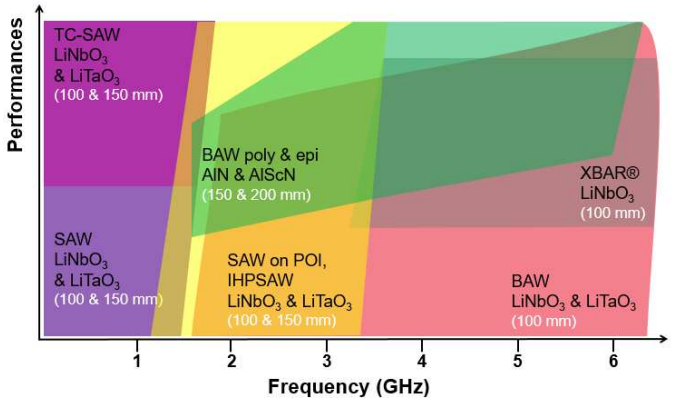

Fig. 1. Acoustic filters classification.

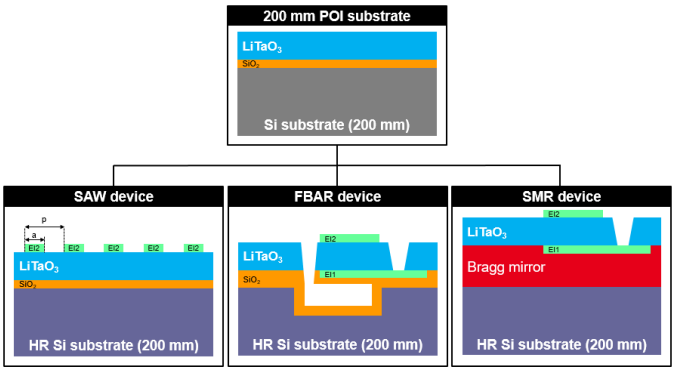

Fig. 2. Schematic cross-sectional view of 200 mm acoustic devices based on POI substrate.

II. 200 mm Surface Acoustic Wave Resonators (SAW)

Single-port synchronous resonators based on 200 nm-thick AlSi interdigitated electrodes with a pitch of 1.2 µm (a/p=0.5) patterned by using standard UV-photolithography and dry etching were used to extract SAW characteristics on 200 mm POI wafers with a 680 nm-thick Y+42° $LiTaO_3$ piezoelectric layer (Fig. 3a, b). They exhibit an electromechanical coupling coefficient of 8.8% at 1.6 GHz (Fig. 3c), which is comparable to the performances previously reported for 150 mm POI substrates [2] and thus validates that the wafer scaling did not degrade the substrate quality and also the RF performances.

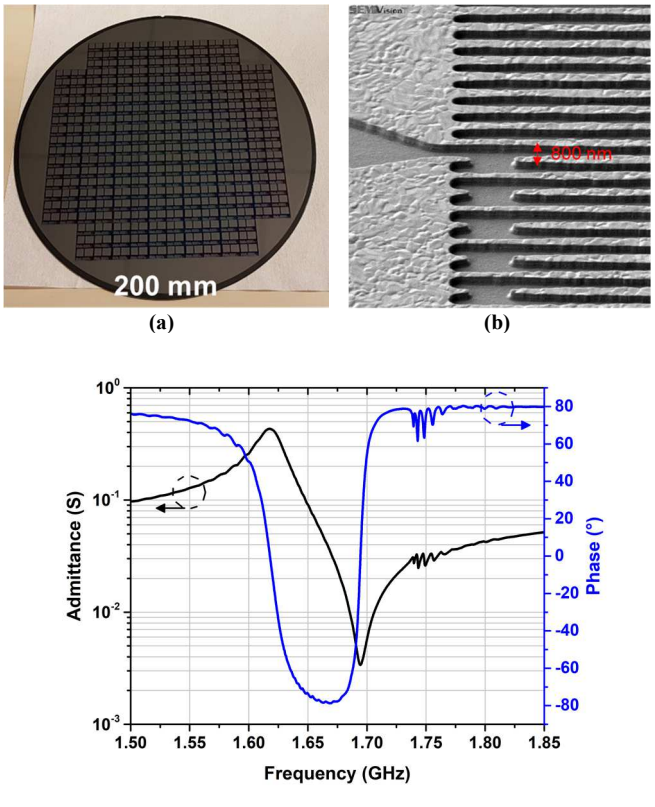

Fig. 3. (a) 200 mm SAW device based on POI, (b) SEM images of final IDTs, (c) Modulus (black) and phase (blue) of the admittance of the tested single-port resonator near 1.6 GHz.

III. 200 mm Bulk Acoustic Wave (BAW) Resonators

For a first demonstration of the capability to employ 200 mm POI wafers for BAW devices, we considered the same wafers as for SAW devices. Y+42°-cut $LiTaO_3$ promotes a pure longitudinal bulk wave with an electromechanical coupling coefficient of 9.0%, similar to AlScN [12].

A. Film Bulk Acoustic Wave Resonator (FBAR)

The fabrication of FBAR-based POI devices is illustrated in Fig. 4a [14]. Two wafers are involved: (1) a "top" (or donor) wafer, which is the POI wafer, and (2) a "base" (or handling) wafer, which is a double-side polished high-resistivity Si wafer. After substrate cleaning, a 100 nm-thick Pt layer is sputtered on the "top" wafer and patterned by Ion Beam Etching. 1 µm-thick sacrificial layer cavities are defined using photolithography and Reactive Ion Etching of the "base" wafer. After photoresist stripping, a 500 nm-thick thermal oxide is grown. Then a 1.5 µm-thick LPCVD poly-Si is deposited to fill the cavities, followed by a selective chemical mechanical polishing (CMP) where the thermal oxide serves as a stop layer. SiO_2 layers are subsequently deposited on both "donor" and "top" wafers and prepared for room temperature hydrophilic bonding. After bonding, the back side of the "top" wafer is removed by grinding and wet etching.

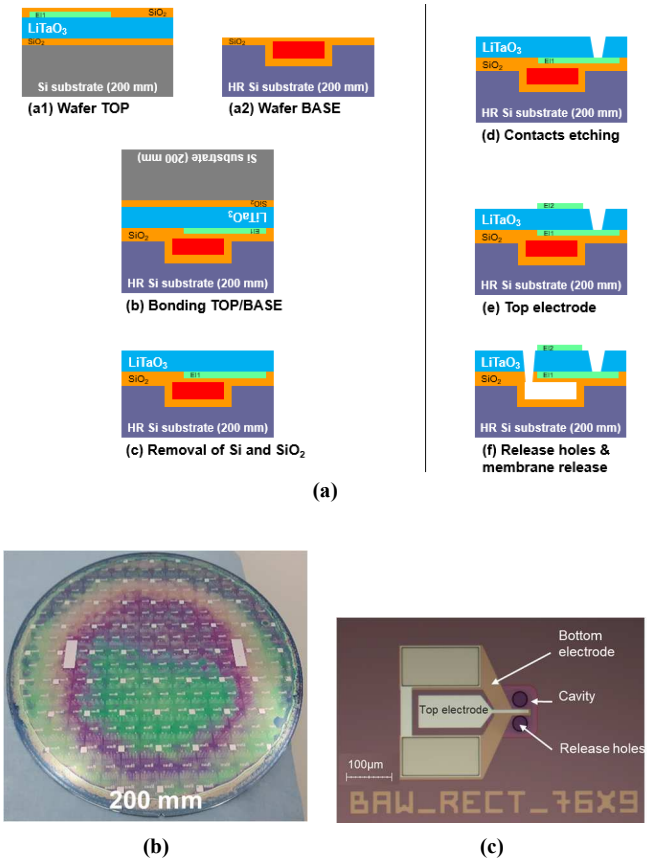

Fig. 4. (a) Process flow for 200 mm FBAR based on POI, (b) photograph of a wafer after fabrication, and (c) optical micrograph of a single resonator.

Electrical contacts to the bottom electrodes and release holes giving access to the sacrificial layer are then etched by ion beam etching. An AlSi top electrode is sputtered and patterned by wet etching. Membranes are finally released by etching the poly-Si sacrificial layer with gaseous XeF_2 (Fig. 4b, c).

The FBAR stack is as follows (from top to bottom): AlSi 100 nm / Y+42°-cut $LiTaO_3$ 630 nm / Pt 100 nm / SiO_2 350 nm. Fig. 5a presents a typical admittance curve and reveals resonance and antiresonance frequencies of respectively 2.82 and 2.97 GHz, leading to an electromechanical coupling coefficient of 8.8%. Quality factors at resonance and antiresonance are respectively 190 and 120. The Bode-quality factor reaches a maximum of 200 (Fig. 5b). A comparison of the electric response with Mason's model (Fig. 5a, dashed blue curve) indicates an excellent agreement confirming that the intrinsic coupling coefficient (k^2_{int} = 9.0%) of the film is in line with theoretical expectations for the bulk material. The discrepancy between the fitted mechanical quality factor (Q_{int} = 300), *i.e.* free of the contribution of electrical losses, and quality factor at resonance is primarily due to resistive losses due to Pt bottom electrodes [12].

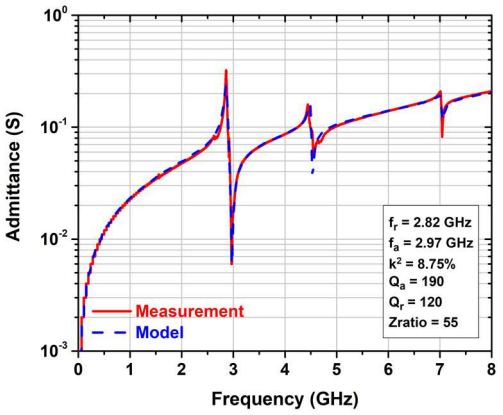

(a)

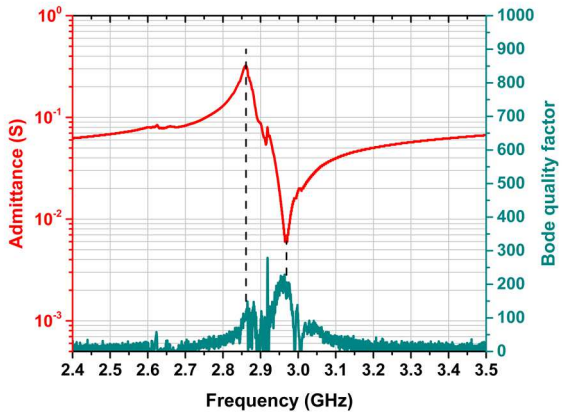

(b)

Fig. 5. (a) Typical response of a Y+42°-cut $LiTaO_3$ FBAR (continuous red curve) and fit of the electric response (Mason's model, dashed blue curve), and (b) comparison between the measured admittance (red) and the calculated Bode quality factor (green).

B. Solidly Mounted Resonator (SMR)

Solidly Mounted Resonators, based on a nine layers Bragg mirror alternating high acoustic impedance (AlN) and low acoustic impedance (SiO_2) layers, were also fabricated.

The SMR stack is as follows (from top to bottom): AlSi 100 nm / Y+42°-cut $LiTaO_3$ 680 nm / AlSi 100 nm / (AlN/SiO_2) Bragg mirror. As illustrated by Fig. 6, the mirror is centered around 4 GHz and is designed to reflect both longitudinal and shear waves [15] as well as to ensure that the main resonance mode is laterally energy-trapped inside the resonator.

The dispersion curves for modes in this stack are calculated using periodic Finite-Element modal analyses (Fig. 7). They indicate a type I dispersion, ensuring an energy trapping configuration [15].

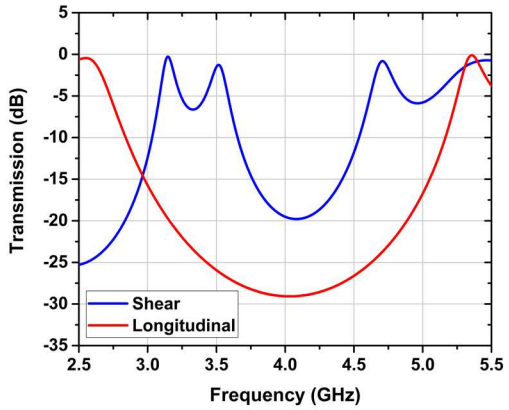

Fig. 6. Transmission coefficient of the designed (AlN/SiO_2) Bragg mirror.

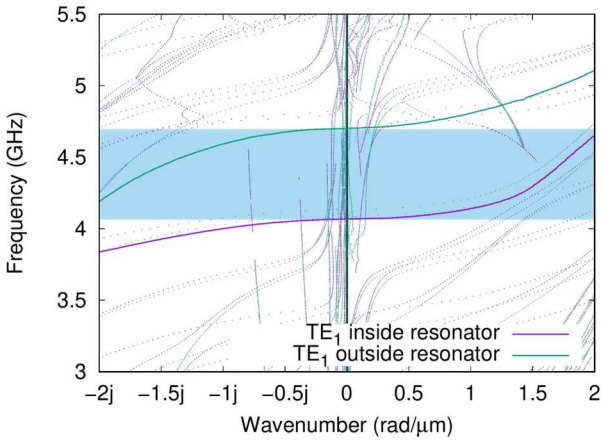

Fig. 7. Dispersion curves of the Y+42°-cut $LiTaO_3$ SMR device.

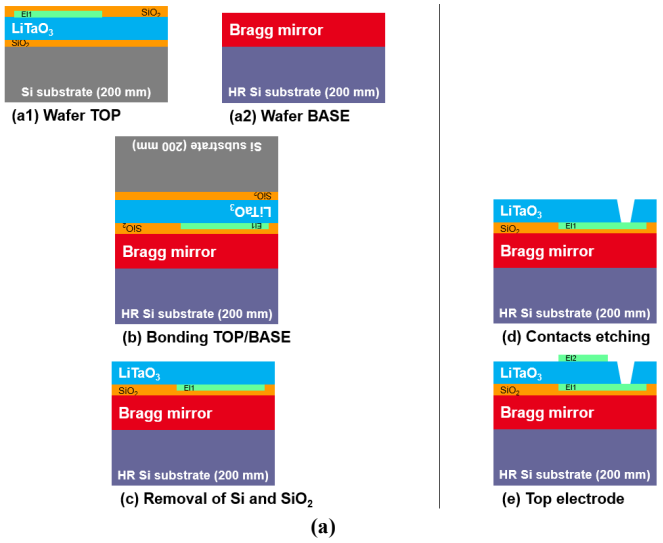

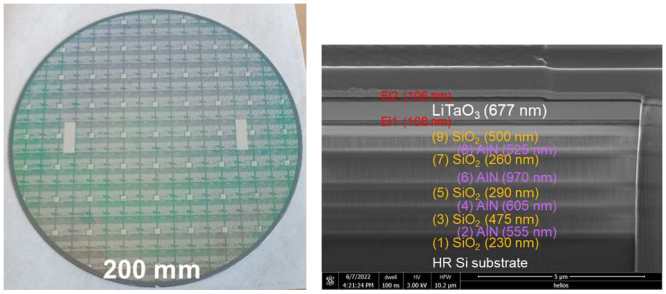

Fig. 8. (a) 200mm SMR-based POI fabrication process, (b) photograph of a wafer after fabrication, and (c) cross-sectional view of the SMR.

Fig. 8a presents the main steps of the fabrication of SMR-based POI devices. The AlN/SiO_2 Bragg mirror is formed on the 200 mm "base" HR Si wafer. SiO_2 and AlN layers are deposited by chemical vapor deposition and physical vapor deposition, respectively. The whole deposition process has been optimized to minimize stress while providing a flat and smooth surface. The last SiO_2 layer also serves as a bonding layer. As for the FBAR device, the top wafer is made of a POI with patterned bottom electrodes (here 100 nm-thick AlSi) and a planarized SiO_2 layer. After bonding and removal of the back side of the top wafer, electrical contacts to the bottom electrodes are then etched by ion beam etching. An AlSi top electrode is sputtered and patterned by wet etching (Fig. 8b, c).

From the spacing between resonance (f_r = 4.03 GHz) and antiresonance (f_a = 4.14 GHz) frequencies, an electromechanical coupling coefficient of 6.1% is calculated (Fig. 9a). This number is mostly limited by the design of the Bragg reflector. The quality factors at resonance and antiresonance are equal to 405 and 235, respectively. Fitting the electric response with a Mason's model allows estimating an intrinsic electromechanical coupling coefficient and quality factor of 7.1% and 300, respectively (Fig. 9a). A Q_{Bode} of 400 and an impedance ratio of 175 (45 dB) are obtained (Fig. 9b).

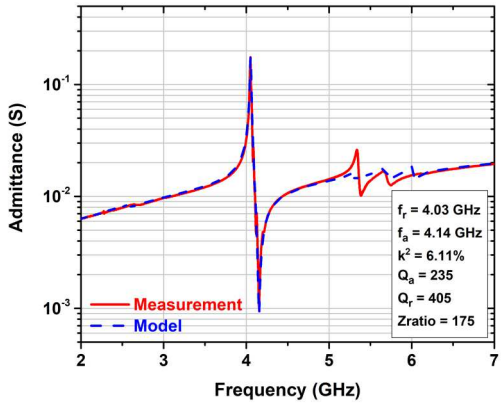

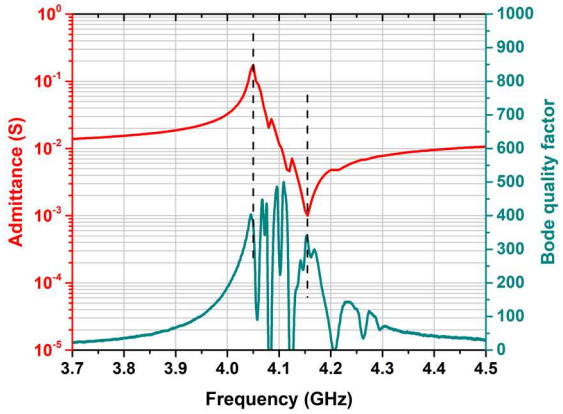

Fig. 9. (a) Typical response of a Y+42°-cut $LiTaO_3$ SMR (continuous red curve) and fit of the electric response (Mason's model, dashed blue curve) and (b) comparison between the measured admittance (red) and the calculated Bode quality factor (green).

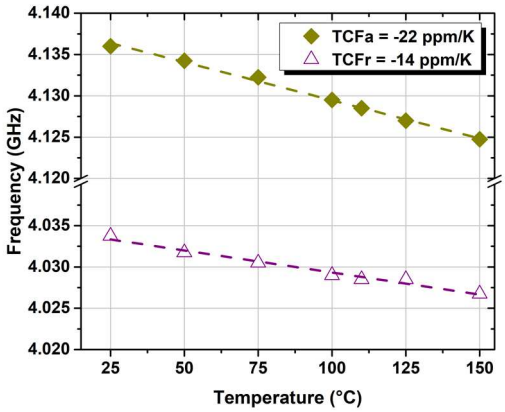

Fig. 10. Temperature coefficient of frequency (TCF) measurements of the 4 GHz Y+42°-cut $LiTaO_3$ SMR device.

TABLE 1. COMPARISON OF TCF VALUES OF $LiNbO_3$ AND $LiTaO_3$ BAW DEVICES.

Ref	BAW device	TCF_a (ppm/K)	TCF_r (ppm/K)
Present work	Y+42°-cut $LiTaO_3$ SMR	-22	-14
[13]	Y+37°-cut $LiTaO_3$ SMR	-37	-23
[12]	X-cut $LiTaO_3$ FBAR	-42	+16
[8]	Y+163°-cut $LiNbO_3$ FBAR	-45	-60
[9]	Y+36°-cut $LiNbO_3$ FBAR	-54	-60
[7]	X-cut $LiNbO_3$ FBAR	-81	-105
[11]	Y+36°-cut $LiNbO_3$ SMR	+55	-108

Finally, the temperature dependence of the $LiTaO_3$ SMR was investigated in the 25°C to 150°C range (Fig. 10). The resonators exhibit a linear frequency shift with temperature, with temperature coefficients of respectively -22 and -14 ppm/K for the resonance and antiresonance. These TCF values are the lowest reported up to now for $LiNbO_3$ and $LiTaO_3$ BAW resonators (Table 1).

IV. CONCLUSIONS

200 mm surface and bulk acoustic devices based on a POI substrate have been successfully fabricated and exhibit performances in agreement with similar devices fabricated from 4-inch wafers. Such 200 mm integration paves the way towards the development of POI ($LiTaO_3$ and $LiNbO_3$) SAW and BAW filters compliant with 5G requirements.

ACKNOWLEDGMENT

This work was partially supported by the French Public Authorities within the frame of IPCEI/Nano2022 project. The authors gratefully acknowledge the contributions from Soitec, CEA-Leti and Substrate innovation center teams to the development of Smart Cut™ POI technology.

REFERENCES

[1] R. Aigner, G. Fattinger, M. Schaefer, K. Karnati, R. Rothemund, and F. Dumont, "BAW Filters for 5G Bands", in Proceedings of the 2018 IEEE International Electron Devices Meeting, pp. 14.5.1-14.5.4.

[2] E. Butaud *et al.*, "Innovative smart cut™ piezo on insulator (POI) substrates for 5G acoustic filters," in Proceedings of the 2020 IEEE International Electron Devices Meeting, pp. 34.6.1-34.6.4..4.

[3] V. Plessky, S. Yandrapalli, P.J. Turner, L.G. Villanueva, J. Koskela, and R.B. Hammond, "5GHz laterally-excited bulk-wave resonators (XBARs) based on thin platelets of lithium niobate," Electron. Lett., vol. 55, pp. 98-100, 2019.

[4] S. Yandrapalli, S. E. Kuçuk Eroglu, J. Mateu, C. Collado, V. Plessky, and L. Guillermo Villanueva, "Towards a N77 Electroacoustic Filter Using Thin Films of Crystalline Y-cut Lithium Niobate," in Proceedings of the 2021 IEEE MTT-S International Microwave Filter Workshop, pp. 112-114.

[5] V. P. Plessky, J. Koskela, and S. Yandrapalli, "Crystalline Y-cut Lithium Niobate Layers for the Bulk Acoustic Wave Resonator (YBAR)," in Proceedings of the 2020 IEEE International Ultrasonics Symposium, pp. 1-4.

[6] M. Bousquet *et al.*, "4.2 GHz $LiNbO_3$ Film Bulk Acoustic Resonator," in Proceedings of the 2021 IEEE International Ultrasonics Symposium, pp. 1-4.

[7] M. Gorisse *et al.*, "High Frequency $LiNbO_3$ Bulk Wave Resonator," in Proceedings of the 2019 IEEE International Frequency Control Symposium & European Frequency Time Forum, pp. 1-2.

[8] M. Bousquet *et al.*, "Single-mode high frequency $LiNbO_3$ Film Bulk Acoustic Resonator," in Proceedings of the 2019 IEEE International Ultrasonics Symposium, pp. 84-87.

[9] A. Reinhardt *et al.*, "Lithium Niobate Film Bulk Longitudinal Wave Resonator," in Proceedings of the 2021 IEEE International Frequency Control Symposium & European Frequency Time Forum, pp. 1-4.

[10] L. Lv, Y. Shuai, S. Huang, D. Zhu, Y. Wang, W. Luo, C. Wu, and W. Zhang, "BAW Resonator with an Optimized SiO_2/Ta_2O_5 Reflector for 5G Applications," ACS Omega, vol. 7, pp. 20994−20999, 2022.

[11] M. Kadota, M. Kadota, F. Yamashita, and S. Tanaka, "4 and 7 GHz solidly mounted thickness extension mode bulk acoustic wave resonators using 36°Y $LiNbO_3$," Jpn J. Appl. Phys., vol. 62, art. no SJ1004, 2023.

[12] M. Bousquet *et al.*, "Potentialities of $LiTaO_3$ for Bulk Acoustic Wave Filters," in Proceedings of the 2020 IEEE International Ultrasonics Symposium, pp. 1-4.

[13] M. Kadota, Y. Ishii, and S. Tanaka, "3.4 GHz strip-type thickness shear mode solidly-mounted bulk acoustic wave resonator using X-cut $LiTaO_3$," Jpn J. Appl. Phys., vol. 61, art. no. SG1041, 2022.

[14] M. Bousquet, P. Perreau, and A. Reinhardt, "Process for fabricating a component comprising a layer made of single-crystal material compatible with high thermal budgets," US Patent application 2022/0166398 A1.

[15] S. Marksteiner, J. Kaitila, G. G. Fattinger, and R. Aigner, "Optimization of acoustic mirrors for solidly mounted BAW resonators," in Proceedings of the 2005 IEEE International Ultrasonics Symposium, pp. 329-332.